

In situ reflection high energy electron diffraction study of dehydrogenation process of Pd coated Mg nanoblades

F. Tang,^{a)} W. Yuan, T.-M. Lu, and G.-C. Wang

Department of Physics, Applied Physics and Astronomy, Rensselaer Polytechnic Institute, Troy, New York 12180-3590, USA

(Received 23 March 2008; accepted 11 June 2008; published online 12 August 2008)

The near surface structural evolution in dehydrogenation process of air exposed Pd coated Mg nanoblades was characterized *in situ* from room temperature to ~ 573 K using reflection high energy electron diffraction (RHEED). The evolved normalized diffraction intensity and the full width at half maximum of diffraction peaks have been correlated with the growth of crystal and the change in crystal size, respectively. With RHEED, we are able to detect crystal sizes smaller than ~ 2 nm. At room temperature the dominant structures near surface were Pd and MgH_2 . With the substrate heating MgH_2 started to gradually decompose at ~ 380 K. When the temperature increased to ~ 480 K MgH_2 was nearly depleted and Mg_6Pd alloys started to form. In addition, at high temperatures pure Mg reappeared and MgO was enhanced significantly even in high vacuum condition. We have discussed the effect of Mg oxide on the dehydrogenation process and the alloy formation between Pd and Mg as well as the accompanying migration of Mg to the surface at high temperatures. Based on our experimental results the structures and compositions that limit the hydrogenation/dehydrogenation cycle of Pd coated Mg nanoblades are suggested. Our findings can help the design of future recyclable hydrogen storage materials. © 2008 American Institute of Physics. [DOI: 10.1063/1.2967735]

I. INTRODUCTION

The depletion of fossil fuels and the global warming effect have tremendously increased the demands for renewable and clean energy resources.^{1,2} Hydrogen has been considered as one of the promising alternative energy resources due to its abundance and high energy density.¹ However, to realize a hydrogen economy, there still remain a number of scientific and technical issues. The storage of hydrogen has been identified as a central concern, especially in the on-board application to automobiles.¹

The pursuit of materials for hydrogen storage has generated intense experimental and theoretical activities. Some key criteria for the storage materials are: weight percentage of hydrogen absorption in the host material, fast kinetics for hydrogen adsorption and release, low hydrogen desorption temperature, and lifetime of hydrogenation and dehydrogenation cycling. Hydrogenation/dehydrogenation processes in solids are usually complicated. Many factors such as the size of materials (nanoscale or microscale),³ the catalyst,⁴ the crystallinity of host materials,^{5,6} the oxides,⁷ etc., have shown to play roles in improving the hydrogen kinetic properties and lowering the desorption temperature. The diffraction technique has been demonstrated as one of the most powerful tools revealing structural evolution in the hydrogenation/dehydrogenation processes. Examples are (1) hydrogen desorption in mechanically milled MgH_2 –5 at. % Nb powders where the metastable phase of Nb hydride was found to exist and it acts as a gateway for hydrogen release from MgH_2 using *in situ* time resolved x-ray scattering with advanced photon source;⁸ (2) the study of

structures and kinetics of dehydrogenation of air exposed ball milled $\text{MgH}_2/\text{Mg}_2\text{Cu}$ and $\text{MgH}_2/\text{MgCu}_2$ using *in situ* x-ray powder diffraction where alloying of Mg with Cu was found to improve kinetics by weakening the H bonds as well as the resistance to surface oxidation;⁹ and (3) *in situ* neutron diffraction of hydrogenation/dehydrogenation of Mg–Nb nanocomposite where the metastable Nb hydride is believed to trigger rapid H desorption.¹⁰ In the above mentioned systems, the Mg hydride was either created from mechanically milling of MgH_2 powder^{8,9} or by hydrogenation at high temperature (>573 K).¹⁰ The crystal size of the hydride is usually large with a typical size of more than ~ 8 nm.¹¹ The corresponding dehydrogenation of the systems also occurred at a high temperature (>573 K). In contrast, Pd coated/doped Mg thin films have been demonstrated with significant hydrogenation/dehydrogenation at a temperature of less than 373 K.^{5,12–16} At this low temperature, Mg hydride has a very small crystal size of a few nanometers. These small crystallites cannot be effectively measured by the conventional x-ray diffraction (XRD). In practice for a crystal with size of less than ~ 4 nm, its structure may show up as virtually amorphous phase in XRD.^{16,17}

In this paper, we present a fresh approach that uses near surface sensitivity of reflection high energy electron diffraction (RHEED) instead of x-ray or neutron diffraction to study the air exposed hydrided Pd coated Mg nanoblades. Despite multiple scattering of electrons, RHEED has the advantage of fast data acquisition and compatibility with deposition of thin films in a vacuum.¹⁸ More importantly, due to the large scattering cross section between electrons and materials, RHEED can reveal very fine crystal structure with size of less than ~ 2 nm.¹⁹ Our Mg nanoblade sample was grown by oblique angle deposition with a blade thickness of

^{a)}Author to whom correspondence should be addressed. Electronic mail: tangf2@rpi.edu.

less than ~ 30 nm. This nanostructure is an ideal sample for RHEED that has a few nanometer probing depth; therefore, RHEED can transmit through and reveal the near surface phase, which is a significant portion of the volume in such ultrathin Mg nanoblades. We chose Pd as a catalyst to dissociate hydrogen molecules during hydrogenation.¹⁵ Through our RHEED study, the detailed structure evolution, such as the MgH_2 depletion, PdMg alloy formation, and continuous MgO growth, has been explored during the dehydrogenation process of the air exposed hydrided Pd coated Mg nanoblades. These findings may help in designing the hydrogen storage nanomaterials with repeatable hydrogenation and dehydrogenation cycling.

II. EXPERIMENTS

The Pd coated Mg nanoblades were prepared in an ultrahigh vacuum chamber equipped with two thermal evaporation sources: Mg and Pd. The Mg nanoblades on the oxide covered Si substrate were grown under oblique incident vapor flux of 75° with respect to the substrate normal.^{20,21} During Pd coating, the incident Pd flux was nearly normal to the substrate or parallel to the vertical standing Mg nanoblades. We swung the substrate within an angular range of $\pm 15^\circ$ with respect to the normal incident Pd flux direction in order to achieve a more uniform Pd coating on both sides of Mg nanoblades. During the growth of Mg and Pd the pressure increased from the base pressure from $\sim 3.0 \times 10^{-9}$ to $(\sim 2.0\text{--}3.0) \times 10^{-8}$ Torr. The evaporation rate of Mg ranged from ~ 9.0 to ~ 12.0 nm/min as indicated by a quartz crystal monitor (QCM). The Pd growth rate was ~ 0.12 nm/min judging from the reading of the QCM and a total of ~ 6.5 nm Pd was deposited. After the Pd coating, the Mg nanoblade sample was transported by a magnetic linear feedthrough from the evaporation chamber to the reaction chamber by opening an in-line valve that connects these two chambers. The Pd coated Mg nanoblades were hydrogenated in this reaction chamber at a pressure of 1 bar with the substrate temperature held at ~ 333 K for ~ 15 h. The hydrided Pd coated Mg nanoblades were taken out from the reaction chamber and mounted on a sample holder with a heating capability in the RHEED chamber. A W filament heater is fully enclosed within a box made of stainless steel foil in order to avoid leaking of the light from the heater during the RHEED measurements. The pressure in the RHEED chamber was $\sim 2.0 \times 10^{-9}$ Torr after pump down. The RHEED gun was operated at 9 kV primary voltage and 0.2 mA emission current. The RHEED pattern at room temperature was recorded first. Then, the sample was heated up to ~ 573 K at a heating rate of ~ 3 K/min. The RHEED patterns were recorded as a function of time that was converted to temperature through the heating rate. The data collection time for each RHEED pattern was about 1 min.

III. RESULTS AND DATA ANALYSIS

Figure 1 shows the RHEED patterns obtained from hydrided Pd coated Mg nanoblades at 306, 402, 483, and 564 K with the incident electron beam perpendicular to the wider width of the hydrided nanoblades. The inset outlined by a

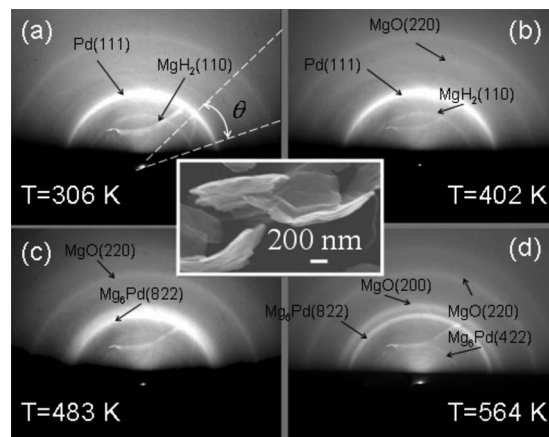


FIG. 1. RHEED patterns from hydrided Pd coated Mg nanoblades at various temperatures: (a) 306 K, (b) 402 K, (c) 483 K, and (d) 564 K. The RHEED patterns were recorded with the incident electron beam perpendicular to the wider width of the hydrided Pd coated Mg nanoblades. The double headed arrow between two dashed lines represents the region used for θ angle average of the diffraction intensity. Diffraction rings from Pd, MgH_2 , MgO, and Mg_6Pd are labeled. The inset outlined by a white bordered rectangle is a SEM top view image of the hydrided Pd coated Mg nanoblades prepared under a similar condition. The incident Mg flux direction in the inset is from top to bottom.

white bordered rectangle in Fig. 1 is a scanning electron microscopy (SEM) top view image of the hydrided nanoblades prepared under a similar condition. The nanoblade became curved after hydrogenation. The RHEED patterns consist of concentric diffraction rings, which are typical transmission diffraction patterns of polycrystalline films.¹⁸ In the transmission model, RHEED measures the protrusions of the nanostructured film and has a near surface sensitivity with a detection depth of a few nanometers.¹⁹ The radius of the rings from the straight through beam is proportional to the reciprocal space distance of particular diffractions. Usually, the reciprocal distance can be calculated by knowing the system parameters such as the sample to phosphorus screen distance and the primary energy of electron beam. However, the large uncertainty in the measurement of distance from the sample to phosphorus screen can yield an error of up to 10% in determining the reciprocal distance.¹⁹ Here, we applied the calibration method similar to XRD measurement.²² Briefly, we mounted a Pt nanorod sample side by side with the hydrided nanoblade sample on the sample holder. Since we know the lattice constant of Pt, 3.93 Å, we can use this value to calibrate the converted reciprocal distance for hydrided nanoblades. Through this calibration, the error in the lattice constant measurement can be reduced to within $\sim 2\%$, which makes the structure determination of specific elements or alloys possible. Diffraction rings from Pd, MgH_2 , MgO, and Mg_6Pd were labeled in the diffraction patterns.

Figure 2 shows the plots of θ angle averaged diffraction intensity (radially averaged intensity in Ref. 19) as a function of reciprocal distance K , obtained from RHEED patterns as shown in Fig. 1. Each data point at a particular reciprocal distance K or radius distance from the straight through spot in a plot was obtained by averaging the diffraction intensity along an arc within the θ angle of $\sim 30^\circ$ range, indicated by the double headed arrow between two dashed lines as shown

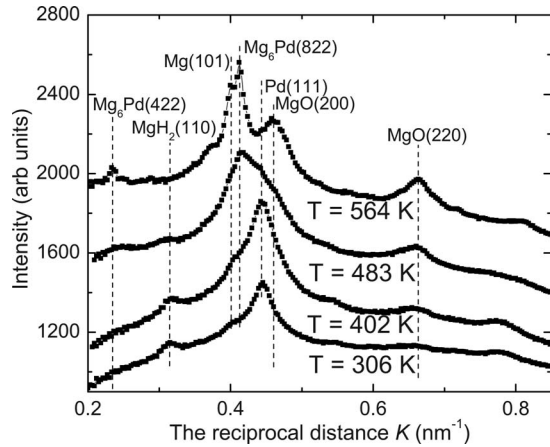


FIG. 2. The plots of θ angle averaged diffraction intensity as a function of reciprocal distance K in units of nm^{-1} at different temperatures: 306, 402, 483, and 564 K. Diffraction peaks from Mg, Pd, MgH_2 , MgO, and Mg_6Pd are labeled.

in Fig. 1(a). This choice avoids the angular range, where the obvious glitches are located in the RHEED patterns. The plotted intensity has been processed by the background subtraction and intensity normalization, which was described in detail in the work of Drotar *et al.*¹⁹ The intensity normalization was carried out by dividing the polar angle average intensity by the background intensity. This step is particularly important because the intensity fluctuation or the drift of the electron beam can be compensated. From the plots we can see that at near room temperature of 306 K, the film consists of Pd and MgH_2 . Within the probing depth of the electron (a few nanometers) the surface indeed has been hydrogenated. The surface also contains MgO, which is not surprising because the sample has been exposed to air when taken out from the hydrogenation chamber and mounted in the RHEED chamber. When the temperature continues to increase, the near surface structures continue to evolve. After the sample was heated to 564 K, MgH_2 was fully depleted. The surface phases were mainly converted to Mg_6Pd and Mg. The amount of Mg oxide was also significantly increased. Using XRD Doménech-Ferrer *et al.*²³ also showed a clear formation of Mg_6Pd phase when the hydrided Pd coated Mg film was dehydrogenated at a temperature of ~ 623 K. This result is consistent with the alloyed phase observed in our RHEED measurement.

For quantitative analysis, we selected three diffraction peaks at various temperatures for peak fit. For example by fitting $\text{MgH}_2(110)$ peak with a Gaussian function at a fixed temperature we can obtain the intensity and the full width at half maximum (FWHM) of that peak. We repeated the fit of the same diffraction peak at various temperatures. Then, we can plot the intensity and FWHM of each peak versus the temperature. In Fig. 3, we show the changes in $\text{MgH}_2(110)$, $\text{Mg}_6\text{Pd}(422)$, and $\text{MgO}(220)$ peaks as the temperature increases. The $\text{MgH}_2(110)$ intensity started decreasing around 380 K and was depleted around 500 K while the FWHM of $\text{MgH}_2(110)$ was almost constant before being completely dehydrogenated. The FWHM of a peak is inversely proportional to the average size of grains, implying that MgH_2 has an average grain size of ~ 5 nm. The alloy phase of Mg_6Pd

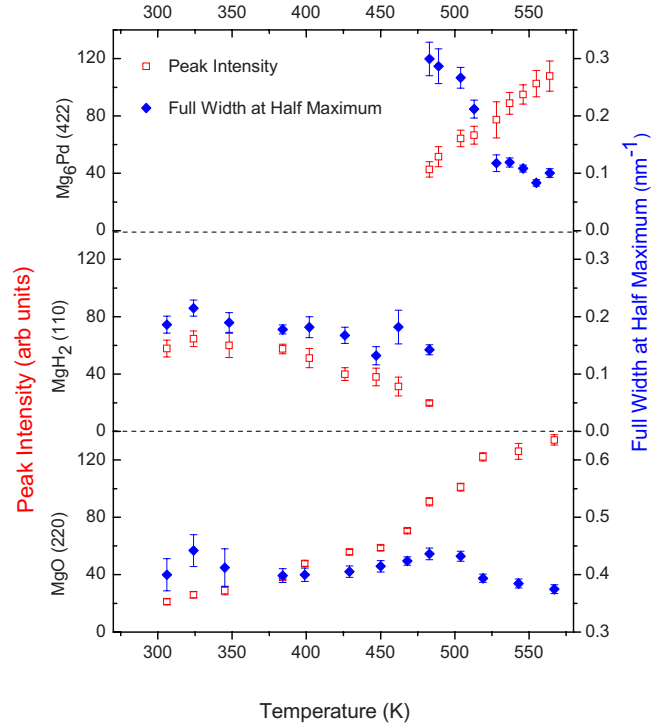


FIG. 3. (Color online) The evolution of the diffraction intensity (open squares) and FWHM (filled diamonds) of $\text{MgH}_2(110)$, $\text{Mg}_6\text{Pd}(422)$, and $\text{MgO}(220)$ as a function of temperature in the dehydrogenation process of hydrided Pd coated Mg nanoblades. The average crystallite size in units of nanometer is the inverse of FWHM.

started to show up at ~ 480 K, indicated by the appearance of the $\text{Mg}_6\text{Pd}(422)$ diffraction intensity. The intensity of alloy diffraction peak increased from ~ 35 to ~ 110 (arbitrary units) with the increasing temperature, whereas the FWHM of the corresponding diffraction peak decreased from ~ 0.3 to ~ 0.1 nm^{-1} with the increasing temperature. Since the amount of detected materials is proportional to the multiplication of FWHM and intensity, this means that although the crystallinity of alloy phase has been enhanced, i.e., the crystal size increased from ~ 3 nm at 480 K to ~ 10 nm at 570 K, the intensity from the detected amount of alloy phase near surface was not sufficiently increased. This observation could be due to the fact¹⁵ that the alloy formation was usually accompanied by the migration of Mg to the top surface. In this case, although the alloy phase was formed and grew, it was buried by Mg layer and the diffraction intensity from alloy phase was attenuated by the Mg layer.

IV. DISCUSSION

The dehydrogenation process started at ~ 380 K as indicated by the decreased diffraction intensity of MgH_2 , as shown in Fig. 3. This temperature is close to the previously reported hydrogen desorption temperature of Pd coated/doped Mg thin films,^{12–14} which is at ~ 373 K. However, instead of a sharp dehydrogenation at ~ 380 K, the amount of MgH_2 in our sample gradually decayed and became fully depleted until reaching a significant higher temperature at ~ 500 K. This could be due to the fact that our sample has been air exposed. It was known^{13,14} that the hydrided Mg film will be partially decomposed in air with a thin layer of

Mg formed between Pd and MgH₂. This Mg layer can be oxidized easily in air due to our noncontinuous Pd coating (observed from transmission electron microscopy (TEM) and electron energy loss spectroscopy, not shown here) on the Mg nanoblade faces, which may have significantly delayed the dehydrogenation process.

It is commonly believed that for the Pd catalyzed Mg system to have a good cyclic hydrogenation/dehydrogenation property, the Mg alloy phase must be avoided. From our RHEED study, a significant dehydrogenation occurred below 480 K before the alloy formation. Krozer and Kasemo¹⁵ showed that at ~353 K, a significant amount of Mg intermixed with Pd. Pd and Mg also formed alloys in the interface region as low as 323 K.^{24,25} Both the reported temperatures are lower than the 480 K obtained from our RHEED measurements. This can be a consequence of the delayed dehydrogenation process, through which enough elemental Mg has to be produced in order to form alloy with Pd. The oxide layer formed during the air exposure is another possible mechanism causing the retarded formation of alloy between Pd and Mg. Researchers²⁶ also argued that alloy formation between Mg and Pd may play an important role to lower the hydrogen desorption temperature of MgH₂. From our experimental results, the alloy formation only became obvious when most of MgH₂ was depleted. This suggests that the alloy formation may not be the mechanism for lowering the hydrogen desorption temperature of MgH₂ in Pd catalyzed Mg system.

Another interesting observation in the structure evolution is the continuous MgO growth in the vacuum during the substrate heating. As shown in Fig. 3, the intensity of MgO(220) resulted from the air exposure continually increasing from room temperature up to 570 K while the average grain size slightly increased from ~2 nm at room temperature to ~3 nm at 570 K. The Mg oxide developed more rapidly above ~480 K, where the MgH₂ has been sufficiently decomposed. Through the x-ray photoelectron spectroscopy (XPS) study, Friedrichs *et al.*²⁷ showed the formation of amorphous layers of Mg(OH)_x on the surface of MgH₂ particles during air exposure. The MgO could be produced during the dehydrolyzation of Mg(OH)_x when the substrate was heated.²⁸ However, we also cannot exclude the possible oxidization of Mg from the adsorbed oxygen on the surface during air exposure and the residue oxygen gas in the vacuum chamber. During the substrate heating, the highest pressure had increased to medium 10⁻⁸ Torr. The MgO layer formed on the surface will introduce the extra barrier for H atom diffusion,²⁹ reducing hydrogen desorption kinetics and storage cycling ability.

Accompanying the phase changes, shifts of the binding energy in chemical bonds among the elements may also occur. An XPS study of these binding energy shifts will provide complementary information about the phase changes, which warrants further investigation.

V. CONCLUSION

In summary, from the RHEED pattern analysis we observed various phase changes with sizes in the range of a few

nanometers near the surface region of hydrided Pd coated nanoblades during the dehydrogenation process. It reveals the depletion of MgH₂ around ~480 K, the alloy formation between Pd and Mg as well as the accompanying migration of Mg to the surface for temperature >480 K. To enhance the cycling ability of the Pd catalyzed Mg system, the dehydrogenation temperature has to be kept below ~480 K for air exposed samples. Also, it shows a significant oxide growth during the dehydrogenation. A continuous Pd coating will be necessary in order to prevent the oxidization of Mg.

ACKNOWLEDGMENTS

F.T. was supported by the NSF under Award No. 0506738. We thank T. Parker for his technical support for hydrogenation experiments.

- ¹L. Schlapbach and A. Züttel, *Nature (London)* **414**, 353 (2001).
- ²W. Grochala and P. P. Edwards, *Chem. Rev. (Washington, D.C.)* **104**, 1283 (2004).
- ³R. W. P. Wagemans, J. H. V. Lenthe, P. E. D. Jongh, A. J. V. Dillen, and K. P. D. Jong, *J. Am. Chem. Soc.* **127**, 16675 (2005).
- ⁴S. Li, P. Jena, and R. Ahuja, *Phys. Rev. B* **74**, 132106 (2006).
- ⁵K. Higuchi, H. Kajioka, K. Toiyama, H. Fujii, S. Orimo, and Y. Kikuchi, *J. Alloys Compd.* **293**, 484 (1999).
- ⁶R. Kelekar, H. Giffard, S. T. Kelly, and B. M. Clemens, *J. Appl. Phys.* **101**, 114311 (2007).
- ⁷G. Barkhordarian, T. Klassen, and R. Bormann, *Scr. Mater.* **49**, 213 (2003).
- ⁸J. F. Pelletier, J. Huot, M. Sutton, R. Schulz, A. R. Sandy, L. B. Lurio, and S. G. J. Mochrie, *Phys. Rev. B* **63**, 052103 (2001).
- ⁹A. Adreasen, M. B. Sørensen, R. Burkarl, B. Møller, A. M. Molenbroek, A. S. Pedersen, T. Vegge, and T. R. Jensen, *Appl. Phys. A: Mater. Sci. Process.* **82**, 515 (2006).
- ¹⁰J. Charbonnier, P. d. Rango, D. Fruchart, S. Miraglia, N. Skryabina, J. Huot, B. Hauback, M. Pitt, and S. Rivoirard, *J. Alloys Compd.* **404**, 541 (2005).
- ¹¹A. R. Yavari, J. F. R. d. Castro, G. Vaughan, and G. Heunen, *J. Alloys Compd.* **353**, 246 (2003).
- ¹²K. Higuchi, K. Yamamoto, H. Kajioka, K. Toiyama, M. Honda, S. Orimo, and H. Fujii, *J. Alloys Compd.* **330**, 526 (2002).
- ¹³R. Checchetto, N. Bazzanella, A. Miotello, R. S. Brusa, A. Zecca, and A. Mengucci, *J. Appl. Phys.* **95**, 1989 (2004).
- ¹⁴R. Checchetto, R. S. Brusa, N. Bazzanella, G. P. Karwasz, M. Spagolla, A. Miotello, P. Mengucci, and A. D. Cristoforo, *Thin Solid Films* **469**, 350 (2004).
- ¹⁵A. Krozer and B. Kasemo, *J. Less-Common Met.* **160**, 323 (1990).
- ¹⁶M. Pasturel, M. Slaman, H. Schreuders, J. H. Rector, D. M. Borsa, B. Dam, and R. Griessen, *J. Appl. Phys.* **100**, 023515 (2006).
- ¹⁷X.-D. Wang, K. W. Hipps, J. T. Dickinso, and U. Mazur, *J. Mater. Res.* **9**, 1449 (1994).
- ¹⁸F. Tang, T. Parker, G.-C. Wang, and T.-M. Lu, *J. Phys. D* **40**, R427 (2007).
- ¹⁹J. T. Drotar, T.-M. Lu, and G.-C. Wang, *J. Appl. Phys.* **96**, 7071 (2004).
- ²⁰F. Tang, T. Parker, H.-F. Li, G.-C. Wang, and T.-M. Lu, *J. Nanosci. Nanotechnol.* **7**, 3239 (2007).
- ²¹F. Tang, G.-C. Wang, and T.-M. Lu, *J. Appl. Phys.* **102**, 014306 (2007).
- ²²B. D. Cullity, *Elements of X-Ray Diffraction* (Addison-Wesley, Reading, MA, 1978).
- ²³R. Domènech-Ferrer, M. G. Sridharan, G. Garcia, F. Pi, and J. Rodríguez-Viejo, *J. Power Sources* **169**, 117 (2007).
- ²⁴A. Krozer, A. Fischer, and L. Schlapbach, *Phys. Rev. B* **53**, 13808 (1996).
- ²⁵J. L. Slack, J. C. W. Locke, S.-W. Song, J. Ona, and T. J. Richardson, *Sol. Energy Mater. Sol. Cells* **90**, 485 (2006).
- ²⁶C. W. Ostefeld, J. C. Davies, T. Vegge, and I. Chorkendorff, *Surf. Sci.* **584**, 17 (2005).
- ²⁷O. Friedrichs, J. C. Sa'nchez-Lo'pez, C. Lo'pez-Cartes, M. Dornheim, T. Klassen, R. Bormann, and A. Fernandez, *Appl. Surf. Sci.* **252**, 2334 (2006).
- ²⁸M. J. McKelvy, R. Sharma, A. V. G. Chizmeshya, R. W. Carpenter, and K. Streib, *Chem. Mater.* **13**, 921 (2001).
- ²⁹P. Hjort, A. Krozer, and B. Kasemo, *J. Alloys Compd.* **237**, 74 (1996).